The Characterization of Mip1 DNA Polymerase

Thomas Lucas

Mentor: Whitney Yin

Table of Contents

The Characterization of Mip1 DNA Polymerase

A. Abstract

Mitochondria are the only organelle to possess their own DNA outside of the nucleus. A single polymerase is primarily responsible for the replication and repair of mtDNA. In humans and other animals, this enzyme is known as polymerase gamma (Pol γ) and it is orthologous to Mitochondrial DNA Polymerase 1 (Mip1) from *Saccharomyces cerevisiae.* Mutations in human Pol γ can cause diseases such as Alper's Syndrome, external ophthalmoplegia (PEO), and other mitochondrial pathologies. Yeast has been used to analyze disease associated mutations in hPol γ by utilizing Mip1 as a model to determine the molecular defects leading to the disease phenotype. While Mip1 and hPol γ are orthologous, the Mip1 protein is a functional monomer possessing a unique C-terminal extended (CTE) domain in contrast to hPol γ's functional heterotrimer complex. In this thesis, I investigated the protein structure and mechanism of action of the CTE domain in replication, repair, and drug induced toxicity to further develop Mip1 as a model for hPol γ and mtDNA maintenance in general.

B. Introduction

The study of *Saccharomyces cerevisiae* (*S. cerevisiae* or baker's yeast), while interesting in its own right, has been invaluable for the study of basic cellular processes and genetics. Researchers have used yeast as a model for eukaryotic cell life due to its simple single celled life cycle and ease of genetic manipulation. These studies have uncovered conserved biochemical mechanisms leading to disease as well as the discovery of novel pharmaceuticals[1]. The study of yeast has helped researchers determine the mitochondria's function in the generation of cellular energy currency, adenosine triphosphate (ATP). Mitochondria houses the enzymes required to generate ATP via the electron transport chain and oxidative phosphorylation (OXPHOS). *S. cerevisiae* played a critical role in the 1963 discovery of the mitochondrial genome. Mitochondria are the only organelle to possess a genome outside the nucleus. It was later discovered that the mitochondrial genome exclusively encodes many of the proteins required for OXPHOS[2].

S. cerevisiae was selected as a model organism for the study of mitochondria function, disease, and biogenesis due to its ability to survive without functional mitochondria. Yeast cells are able to survive via anaerobic metabolism by undergoing alcoholic fermentation[3]. Yeast cells grown on a limited carbon food media struggle to produce biomass while performing alcoholic fermentation and results in visibly smaller colonies known as *"petites"* or the *"petite"* phenotype[4,5]. However, contentious "*petite"* colonies can occur when the mitochondria or OXPHOS malfunction. OXPHOS requires proteins from both the nuclear and mitochondrial genomes which means mitochondrial malfunction can be caused by issues in either the mitochondria or nucleus. Colonies

showing the *"petite"* phenotype are therefore further classified into three groups based upon the status of their mitochondrial DNA. *S. cerevisiae* which retain their functional mitochondrial genome are classified as *rho+.* Colonies devoid of mtDNA are classified as *rho*^{0}. Finally, *rho-* cells retain some mtDNA that has been significantly damaged or deleted [6]. These distinctions highlight different causes of the *"petite"* phenotype and can be used to target the mechanisms leading to the mitochondrial disfunction.

There is only one known replicating DNA polymerase found in the mitochondria, which makes it a key suspect in the generation of distinct *rho* phenotypes. In humans, this polymerase is known as DNA polymerase gamma (hPol γ) and in yeast as mitochondrial DNA polymerase 1 (Mip1). Despite being found almost exclusively in the mitochondria, these proteins are nuclear encoded on the POLG and MIP1 genes for humans and yeast respectively. The polymerases are then imported into the mitochondria where they maintain the mitochondrial genome.

The hPol γ structure has been solved revealing a heterotrimer consisting of a core 140KD polymerase protein hPol γA and a dimer of 58KD hPol γB. The hPol γB dimer has no known independent enzyme activity. Instead, hPol γB serves as processivity factor improving all of the enzyme's known functions[7,8]. The crystal structure of this heterotrimer helped identify many of the mechanisms of disease associated mutations and drug induced toxicity[9,10]. In contrast, Mip1 is a functional monomer. When aligned to the hPol γA sequence, Mip1 possess an additional 279 of amino acids at its C-terminus known as the C-terminal extension (CTE) domain. The 279 amino acids found in *S. cerevisiae* are further separated into a region of 104 amino acids largely conserved among the mitochondrial DNA polymerases of fungi, and the final 175 which share no similarity to

any known protein sequence. Currently, no high-resolution structure of the Mip1 protein or its CTE domain exists to shed light on the spatial chemistry underlying Mip1's mechanism of action.

Current research suggests that the primary function of the CTE appears to be the regulation of the polymerase and exonuclease activity of the protein[11]. However, the specific mechanism of action remains unknown. Both hPol γ and Mip1 are high-fidelity polymerases possessing both highly processive polymerase and 3'-5' exonuclease proof reading activity[12,13]. In addition to serving as the primary replicating polymerase for the mitochondrial genome, Mip1 and hPol γ are involved in mitochondrial Base Excision Repair (BER). BER is the primary pathway for repairing oxidative lesions resulting from the reactive oxygen species (ROS) produced as byproducts of the electron transport chain reacting with the mtDNA[14–16].

BER can proceed along two known pathways. The two pathways diverge at the polymerase incorporation step. Short-patch BER (SP-BER) requires the incorporation of the single correct nucleotide at the spot of damage by the repair polymerase. However, SP-BER is insufficient for the repair of lesions larger than a single nucleotide; creating the need for the long-patch (LP) BER pathway. During LP-BER, the polymerase displaces 2-7 nucleotides on the damaged strand during the dNTP incorporation step. Once the polymerase finishes displacing the damaged DNA, flap endonuclease (FEN-1) cuts the displaced damaged DNA flap to allow ligation of the newly synthesized DNA. The multiple dNTP incorporations and the need for an additional protein action makes LP-BER less efficient than SP-BER. The selection of which method to use in not fully understood, but appears to be influenced by the type of damage and intermediates generated during the

process[17]. The conserved amino acid sequence between Mip1 and hPol γ combined with the limited number of proteins known to be involved in mtDNA maintenance suggest some of the molecular mechanisms must be conserved between humans and yeast[18]. Therefore, the study of BER pathway selection and action in Mip1 should apply, at least in part, to the mitochondria of humans.

Sequence alignment of the core polymerase domains of hPol γ and Mip1 demonstrated highly conserved identity. Specifically, the two proteins are identical in the region known as the O-helix as shown in Figure #1. The O-helix is responsible for ensuring the base pair matching of incoming nucleotides to the DNA template. This region has been determined to be the primary source of drug induced mitochondrial toxicity seen in patients treated with nucleoside reverse transcriptase inhibitors (NRTIs). NRTIs were developed to treat HIV and have been shown to improve outcomes in treat certain cancers[19,20]. They function by mimicking incoming dNTPs used in DNA synthesis but lacking in a 3' hydroxyl group. The missing 3' OH prevents the incorporation of a subsequent dNTP effectively terminating DNA synthesis[21]. Unfortunately, NRTIs often get misincorporated by hPol γ. The limited DNA repair mechanisms found in the mitochondria struggle to remove these bases once misincorporated; resulting in the mitochondrial toxicity seen in some patients[22,23]. The identity between Mip1 and hPol γ has already been used to validate and model pathological mutation found in hPol γ, determine the enzyme defects caused by those mutations, and examine the effects specific drugs have on hPol γ and mtDNA toxicity[24]. This thesis expands the Mip1 model system regarding the biochemical mechanisms involved in NRTI induced toxicity.

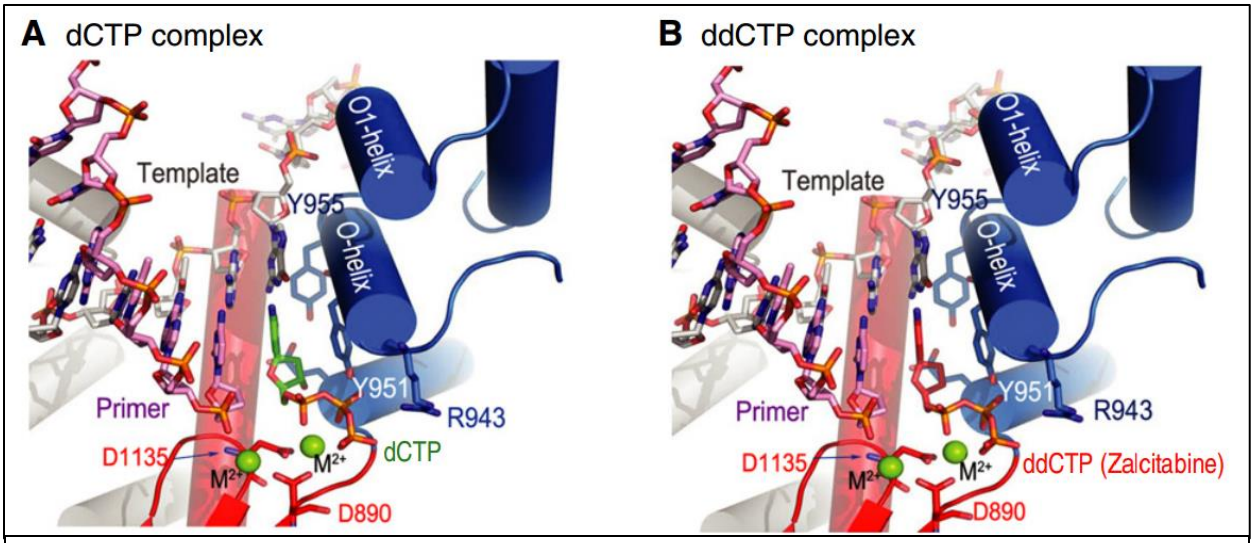


```
                      950        960        970        980        990       1000
PolGammaA      REHAKIFNYGRIYGAGQPFAERLLMQFNHRLTQQEAAEKAQQMYAATKGLRWYRLSDEGE
               :..:::::::::::::  :: .:: .::  ::..:. . :...:  :::
WT_Mip1        RNEAKIFNYGRIYGAGAKFASQLLKRFNPSLTDEETKKIANKLYENTKG----------
                  750        760        770        780        790
```

Figure #1: Image taken from Szymanski et al., 2015 **A** The polymerase active site of a hPol γ ternary complex with a substrate dCTP. **B** The polymerase active site of a hPol γ ternary complex with inhibitor ddCTP (zalcitabine). Amino acid sequence comparison of the human hPol γA to Mip1 using the ALIGN software showed a conserved identity of 27.9%. The region highlighted in green shows the conservation of the O-helix responsible for hPol γ's failure to recognize and discrimination against ddNTP incorporations.

Despite all the similarities between Mip1 and hPol γ, it is important to acknowledge that the mitochondria of yeast and Mip1 possess many unique traits not found in the humans. Understanding these unique characteristics and the mechanisms underlying them is important for the validation of the experiments utilizing *S. cerevesiae* and Mip1 as a model. Unlike mammalian mtDNA which is almost always found in a circular genome, yeast mtDNA can predominantly found in linear tandem arrays[25,26]. The differences in mtDNA structure are significant because they suggest some of the mechanisms for replication or repair of mtDNA in yeast differs from the better characterized mechanisms found in mammals. Mip1 and its unique characteristics are

critical for understanding the source of those differences since Mip1 is responsible for generating all mtDNA.

Mip1 possess three main characteristics that distinguish it from its human ortholog. (1) Mip1 functions as a monomer the size of hPol γA alone, although Mip1 performs the same known functions. Mip1's polymerase and exonuclease activity are regulated by its unique CTE domain, although the precise mechanism is not understood. (2) Mip1's exonuclease site is highly active and will excise even matched DNA[12]. (3) Mip1 is possesses significant strand displacement ability[11]. While some DNA/RNA and repair helicases have been identified in the mitochondria, the ability of Mip1 to strand displace could explained the lack of any identified replicating DNA helicases in the mitochondria of yeast[27,28].

The study of mitochondrial DNA polymerases has become a priority in modern medical science due to hPol γ's involvement in a wide spectrum of disorders from premature aging[29] to certain cancers[30,31], neurological[32,33], cardiovascular[34], and muscular skeletal[35] disorders. This thesis investigates Mip1's role as the primary DNA replicating and repair polymerase for the yeast mitochondrial genome to better understand the processes governing all mitochondrial DNA polymerases. The structural and kinetic experiments explore the similarities between Mip1 and hPol γ to address the gaps in knowledge of the mechanisms of mtDNA repair and drug induced NRTI toxicity. These experiments also investigate Mip1 CTE's potential function as an intramolecular domain and explore its potential role in initiation of mtDNA replication, BER, and NRTI discrimination.

C. Methods

Creation and Expression of Recombinant Mip1 Protein A pBG1805 Gateway® plasmid containing the Mip1 ORF was purchased from Thermo Scientific. SalI and HindIII restriction sites were introduced to the Mip1 ORF and the first 90 NTPs of the mitochondrial localization signal was removed by PCR. The ORF was then cloned into the pET28b plasmid introducing an N-terminal 6x-His tag. The D347A mutation was identified by the Foury lab and selected due to the 500-fold decrease in exonuclease activity[36]. Generation of the exonuclease deficient D347A mutation and the deletion of the C-terminal 175 amino acid was performed by Epoch Life Science. Each expression construct was verified by DNA sequencing.

The plasmids were transformed into *E. coli* Arctic RIL cells (Agilent Technologies). Bacteria were grown to OD_{600} of 0.5 at 30C in Luria Broth containing 10ug/ml of kanamycin at which point the incubation temperature was dropped to 10C. Protein expression was induced by the addition of 0.5mM IPTG and 1mM betaine. Cells were collected after 48hrs of expression at 10C by centrifugation at 8000RPM in a Beckman JA-10 rotor at 4C.

Preparation and Purification of Mip1 All procedures were performed at 4C. Bacteral cell pellets of approximately 2.5g were resuspended in 25mls of buffer containing 25mM HEPES pH 7.5, 1M NaCl, 50mM Betaine, 3mM 2-mercaptoethanol, 0.5% Nonident P-40, 1mg/ml lysozyme, and protease inhibitor cocktail. The cell lysate was incubated for 15mins prior to sonication at 100% cycle, 50% power, 3 x 15seconds. The solution was then cleared via centrifugation for 30mins at 30,000RCF in a Beckman 25.50 rotor. The supernatant was applied to a Ni-NTA gravity column (Qiagen) and washed with 20 column

volumes of buffer containing 10mM imidazole (25mM HEPES pH 7.5, 1M NaCl, 100mM Betaine, 3mM 2-mercaptoethanol). Mip1 was then eluted with 10 column volumes of 100mM imidazole in low salt buffer (25mM HEPES pH 7.5, 150mM NaCl, 100mM Betaine, 3mM 2-mercaptoethanol). Nickel elution was then loaded onto a pre-equilibrated 1ml heparin sepharose (Fischer) affinity column and washed with 20 column volumes of wash buffer (25mM HEPES pH 7.5, 200mM NaCl, 100mM betaine, 3mM 2-mercaptoethanol). Protein was eluted with 10 column volumes of 1M NaCl buffer and fractions were pooled and concentrated with a 50kD MWCO vivaspin 20 (Fischer) to 4ml for gel filtration. Concentrated heparin elution was loaded onto a Hi-Load Superdex 200 gel filtration column (GE Healthcare Life Sciences) and peak fractions were concentrated using 50kd MWCO vivaspin 5. Protein concentration was measured spectrophotometrically using a Nanodrop 2000 (Thermo). Protein purity was assessed via SDS-PAGE analysis and protein aggregation was assessed by dynamic light scattering (DLS, Malvern Micro V Dynamic Light Scattering). All proteins used for these assays were flash frozen in liquid nitrogen and stored at -80C.

BioSAXS analysis: 1mg/ml protein sample was analyzed with a Rigaku BioSAXS-1000. SAXS data was processed with CRYSOL[37] and PRIMUS[38] and a protein surface envelope was generated using the DAMFIT[39] software. The SAXS envelopes were then fitted to the crystal structure of hPol γA for comparison. Images obtained using Pymol software[40].

Preparation of Substrate DNA All DNA constructs used can be found in Table #1. DNA was purchased from Integrated DNA Technologies (IDT). Cy5 labelled DNA was purchased directly from IDT. P32 labeled DNA was generated with T4 polynucleotide

kinase according to manufacturer's instructions (New England Biolabs). Reaction was terminated by incubation at 65C and primer was isolated using a Bio-Spin 6 mini-column (Biorad, Hercules, CA). Labeled DNA primer was combined with template DNA at equi-molar ratio, placed in a water bath at 95C and allowed to anneal by gradually allowing the water to cool to room temperature overnight.

Table #1 DNA Primer/Templates Using in Kinetic Assays
N= variable base depending on the incoming nucleotide
Pre-Steady State Polymerase Assay DNA
5′ /Cy5/ATGACTTGATTTAAGCACTAATACTTACTG 3′ 3′ TACTGAACTAAATTCGTGATTATGAATGACNCGTGCAGTCCGTCC 5′
Pre-Steady State Exonuclease Assay DNA
5′ /Cy5/ATGACTTGATTTAAGCACTAATACTTACC(dd) 3′ 3′ TACTGAACTAAATTCGTGATTATGAATGAGCGTGCAGTCCGTCC 5′
Strand Displacement Assay DNA No Gap
5′ CGCACGTCAGGCAGGCTCGT 3′ 5′ /P32/ATGACTTGATTTAAGCACTAATACTTACTG 3′ 3′ TACTGAACTAAATTCGTGATTATGAATGACGCGTGCAGTCCGTCCGAGCA 5′
Strand Displacement Assay DNA 1-ntp Gap
5′ CGCACGTCAGGCAGGCTCGT 3′ 5′ /P32/ATGACTTGATTTAAGCACTAATACTTACTG 3′ TACTGAACTAAATTCGTGATTATGAATGACGGCGTGCAGTCCGTCCGAGCA 5′
Strand Displacement Assay DNA 2-ntp Gap
5′ CGCACGTCAGGCAGGCTCGT 3′ 5′ /P32/ATGACTTGATTTAAGCACTAATACTTACTG 3′ TACTGAACTAAATTCGTGATTATGAATGACGTGCGTGCAGTCCGTCCGAGCA 5′
Strand Displacement Assay DNA 8-ntp Gap
5′ CGCACGTCAGGCAGGCTCGT 3′ 5′ /P32/ATGACTTGATTTAAGCACTAATACTTACTG 3′ TACTGAACTAAATTCGTGATTATGAATGACGTTCTCTTGCGTGCAGTCCGTCCGAGCA 5′

Strand Displacement Assay DNA 8-ntp Gap with Mismatched 5′ Flap
5′ CGCACGTCAGGCAGGCTCGT 3′ 5′ /P32/ATGACTTGATTTAAGCACTAATACTTACTG 3′ TACTGAACTAAATTCGTGATTATGAATGACGTTCTCTTAAGTGCAGTCCGTCCGAGCA 5′

Pre-Steady State Exonuclease Assays: The 150nM Mip1 protein was pre-incubated on ice in reaction buffer (25mM HEPES, pH 7.5 and 140mM NaCl) containing 1.0mM EDTA for 10mins. 500nM DNA was added to reaction solution and allowed to pre-bind and equilibrate for an additional 20mins on ice. All solutions were then allowed to equilibrate to 30C prior to reaction initiation. Using the Quench Flow RQF-3 (Kin Tek) polymerase activity was measured by rapidly mixing protein/DNA complex with 21mM $MgCl_2$. Final reaction conditions 75nM Mip1 protein, 250nM DNA complex, and 10mM $MgCl_2$. After the designated time, reaction was quenched with buffer containing 85% formamide and 20mM EDTA. Products were run on a DNQ sequencing gel (IBI Scientific). Gel was scanned using a STOMR 860 (GE Life Sciences) system and quantified using the ImageQuant (GE) software. The amount of product formed as a function of time was fit to the burst equation (Equation #1) using the *solver* plug in for Microsoft Excel.

$$\text{Product} = A_0\{1 - e^{-k_{obs}t}\} + v_{ss}\ t$$

Equation #1: The burst equation. A_0 represents the burst amplitude (nM), k_{obs} represents the rate of the polymerase or exonuclease activity (s^{-1}), v_{ss} is the velocity of the steady state, and t represents time (secs).

Pre-Steady State Polymerase Assays: The 150nM Mip1 protein was pre-incubated on ice in reaction buffer (25mM HEPES, pH 7.5 and 140mM NaCl) containing 1.0mM EDTA for 10mins. 500nM DNA was added to reaction solution and allowed to pre-bind and equilibrate for an additional 20mins on ice. All solutions were then allowed to

equilibrate to 30C prior to reaction initiation. Using the Quench Flow RQF-3 (Kin Tek) polymerase activity was measured by rapidly mixing protein/DNA complex with 20mM MgCl2 and 50uM of designated incoming nucleotide corresponding to the DNA template used. Final reaction conditions 75nM Mip1 protein, 250nM DNA complex, 10mM $MgCl_2$, and 50uM (d)dNTP. After the designated time, reaction was quenched with buffer containing 85% formamide and 20mM EDTA. Products were run on a DNA sequencing gel (IBI Scientific). Gel was scanned using a STOMR 860 (GE Life Sciences) system and quantified using the ImageQuant (GE) software. The amount of product formed as a function of time was fit to the burst equation[41] (Equation #1) using the *solver* plug in for Microsoft Excel. Error is reported as standard deviation from replications when available.

The quantification of these results suffered from a significant technical issue that was mistakenly attributed to poor lab techniques. The fluorophore Cy5 was selected in place of flouroscene due to Cy5's increased chemical stability and signal intensity. However, the Cy5 tag can base stack to its DNA molecule and alter the migration of DNA through and electrophoresis gel[42,43]. This phenomenon did not create a problem for labs performing multiple incorporation reactions. However, in a single dNTP incorporation reaction the base stacking could distribute the DNA's signal so that that it was indistinguishable between substrate and product. This often confounded the results and made gel image analysis difficult to impossible. Examples of the distribution of single DNA species signal and the boxing used for quantification can be seen in Figure #2.

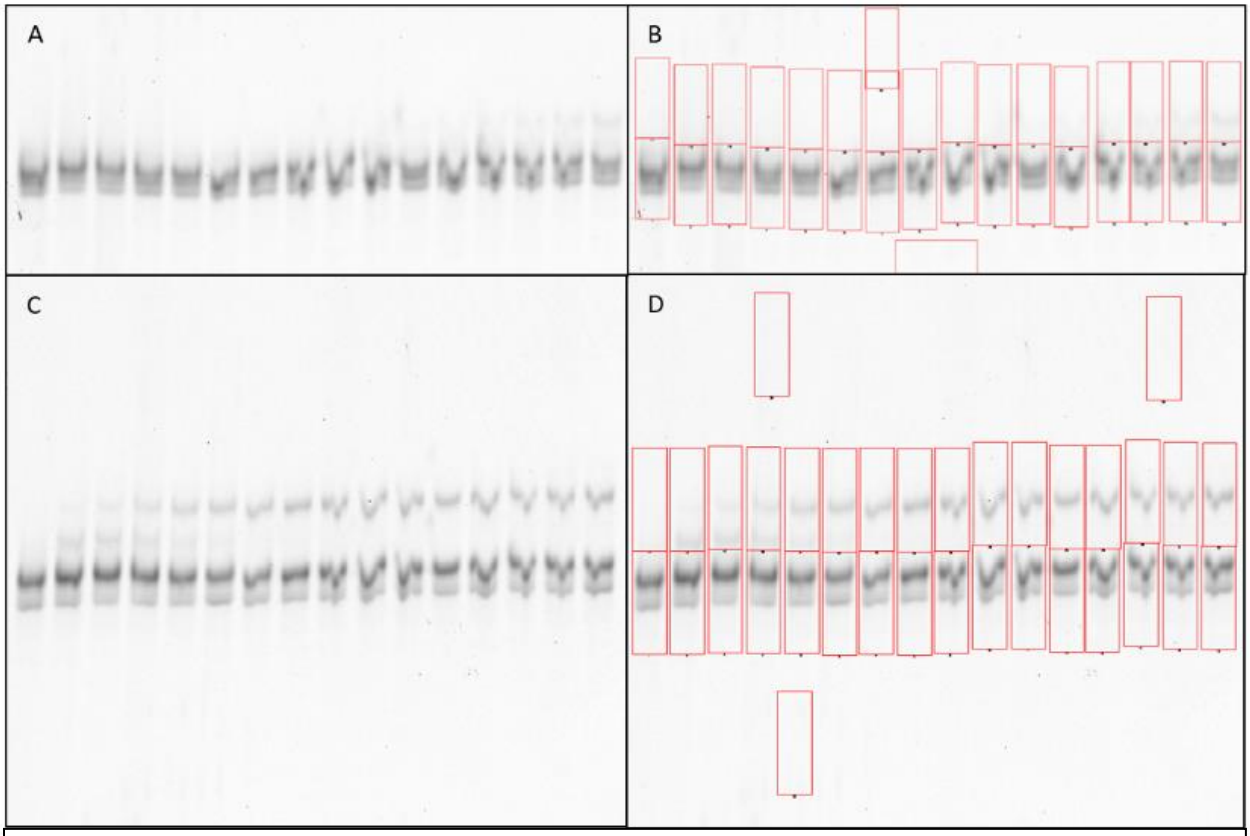

Figure #2: Images of the Cy5 labelled DNA sequencing gel. They show the images of the pre-steady state time courses of Mip1 D347A (A) with incoming ddGTP, (B) boxed for quantification compared to (C) incoming dGTP, (D) boxed for quantification. These samples represent some of the samples with the least Cy5 stacking that allowed for quantification.

Steady State Strand Displacement Activity Assays All reactions were carried out at 30C in buffer contained 25mM HEPES pH 7.5, 140mM NaCl, 0.2mg/ml BSA, and 2mM 2-ME. 50nM Mip1 protein was pre-incubated on ice in buffer containing 0.1mM EDTA for 10mins. 2uM DNA was added to the protein solution and allowed to incubate for an additional 20mins on ice. All solutions were then allowed to equilibrate to 30C. Reaction was initiated by mixing equal volume of nucleotide magnesium solution (100uM dNTP, 20mM $MgCl_2$) with protein/DNA solution. Final reaction conditions 25nM Mip1 protein, 1uM DNA complex, 10mM MgCl2, and 250uM dNTP (when applicable). After the

designated time, reaction was quenched with buffer containing 85% formamide and 20mM EDTA. Products were run on a DNQ sequencing gel (IBI Scientific). Gel was scanned using a STORM 860 (GE Healthcare) system and quantified using the ImageQuant (GE Healthcare) software.

D. Results

Protein expression and purification improved by adding betaine: Replication of the Mip1 purification protocol performed by the Sedman group resulted in a mix of misfolded and truncated protein that was prone to protein aggregation[11]. The small angle x-ray scattering (SAXs) and pre-steady state kinetic assays planned for this thesis required functional protein concentrations that proved to be unattainable by previously reported methods. The new method detailed here improved yields to useable concentrations. The substitution of betaine for glycerol appeared to prevent protein aggregation and precipitation which appeared to be the primary source of protein lose during purification, as evident in Figure #3.

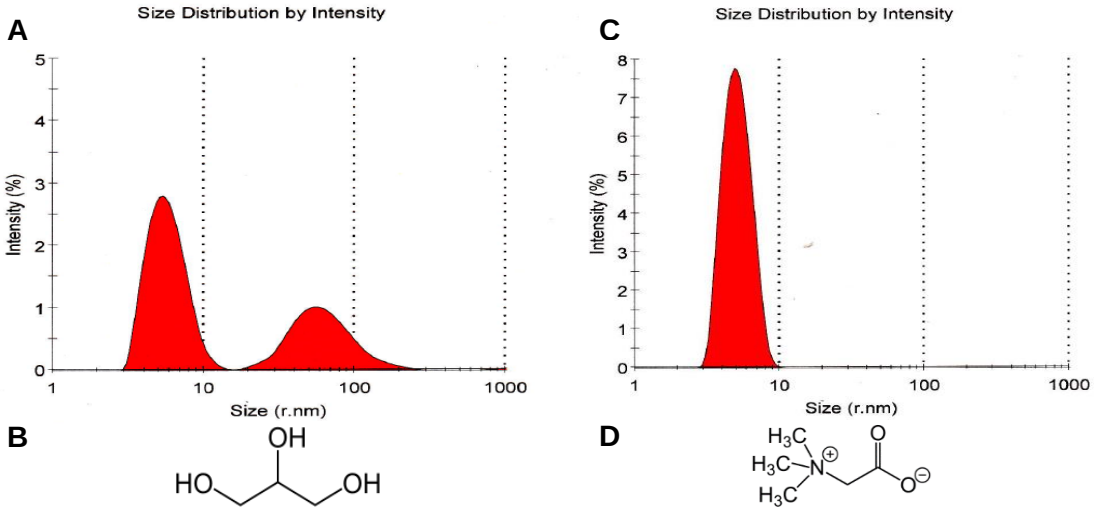

Figure #3: Dynamic light scattering results show the populations distribution by size. **A** Mip1 purified in the presence of glycerol (B) possesses a large aggregate population. **C** Mip1 purified with betaine (D) removes the aggregated population making it suitable for structural and kinetic experiments.

SAXS structural comparison shows that the CTE appears to be a distinct protein domain: The low-resolution data provided by SAXs was used to determine protein size and shape. This data was used to generate a model of Mip1's surface envelope to determine if the CTE existed as a distinct intramolecular protein domain. Combined with the dynamic light scattering results, the low-resolution structure suggests that the CTE is a distinct structural domain largely apart from the core polymerase domain. The SAXs data was then fitted to the crystal structure of the human hPol γA[7] subunit alone shown in Figure #4. Fitting the Mip1 envelope to the entire human hPol γ heterotrimer proved impossible due to the significantly larger volume of the human complex.

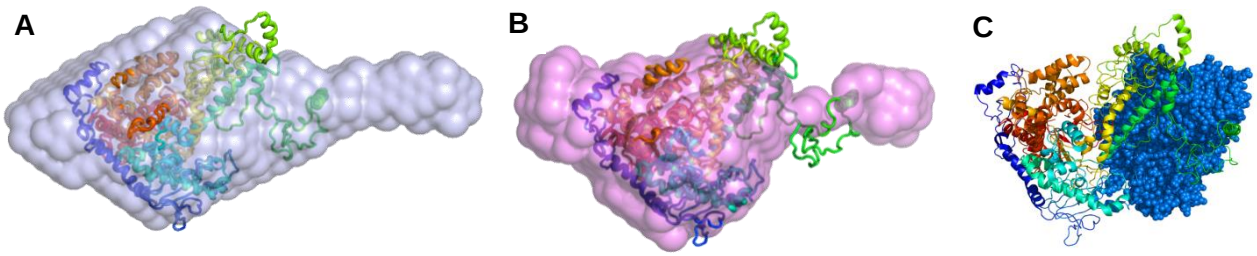

Figure #4: Fitting of the SAXS envelopes of (A) Wt-MIP1 and (B) MIP1d175 to the crystal structure of hPol γA alone. (C) The crystal structure of the hPol γ complex with the B dimer modelled as blue spheres

This fitting shows the position of the CTE aligns with the location of the hPol γ accessory protein domains when the B dimer is returned to the fitted A subunit. The hPol γB dimer has been shown to function as a processivity factor, increasing hPol γA's polymerization rate and affinity for DNA. The CTE of Mip1 appears to have a similar function by regulating the transition between polymerase and exonuclease activities. This evidence suggests the CTE could function similar to the hPol γB dimer despite the difference in amino acid sequence. A high-resolution structure from X-ray crystallography or cryo-electron microscopy of Mip1 bound to DNA is required to confirm this hypothesis.

The Mip1 structure could then be compared to the structure of hPol γ to determine if the CTE interacts with mtDNA through similar spatial chemistry to the hPol γB dimer.

Pre-steady state polymerase assays suggest Mip1's reduced rate of ddNTP incorporation is unaffected by the CTE or exonuclease activity: The initial steady state assay demonstrating Mip1's ability to misincorporate ddCTP is shown in Appendix figure #1 on page 32. The pre-steady state rate of incorporation for dCTP, dGTP, and dATP were compared to those of ddCTP, ddGTP, and ddATP for full-length Mip1 D347A (exonuclease deficient) protein. This experiment assayed the rate (k_{pol}) to determine if it was affected by the removal of the CTE or exonuclease activity. The plot of the results and the resulting burst equation fitting constants are shown in Figure #5 and Table #2 respectively. Each chain terminating ddNTPs appeared to be incorporated at a slower rate than their dNTP counterparts. The result is similar to the hPol γ results where the rate of incorporation by hPol γ is significantly reduced for the NRTI[21,44]. However, hPol γ does not actually discriminate against ddNTPs despite the significant reduction in the rate of incorporation. The reduction in the polymerization rate is counteracted by an increase in the binding affinity of hPol γ. The similarities in the reduction of the k_{pol} of ddNTPs between Mip1 and hPol γ combined with the sequence identity at the critical residues of the O-helix suggest the mechanism causing the ddNTP misincorporation is conserved. Further experiments into the binding of DNA and dNTP would be required to confirm a conserved mechanism of action between hPol γ and Mip1.

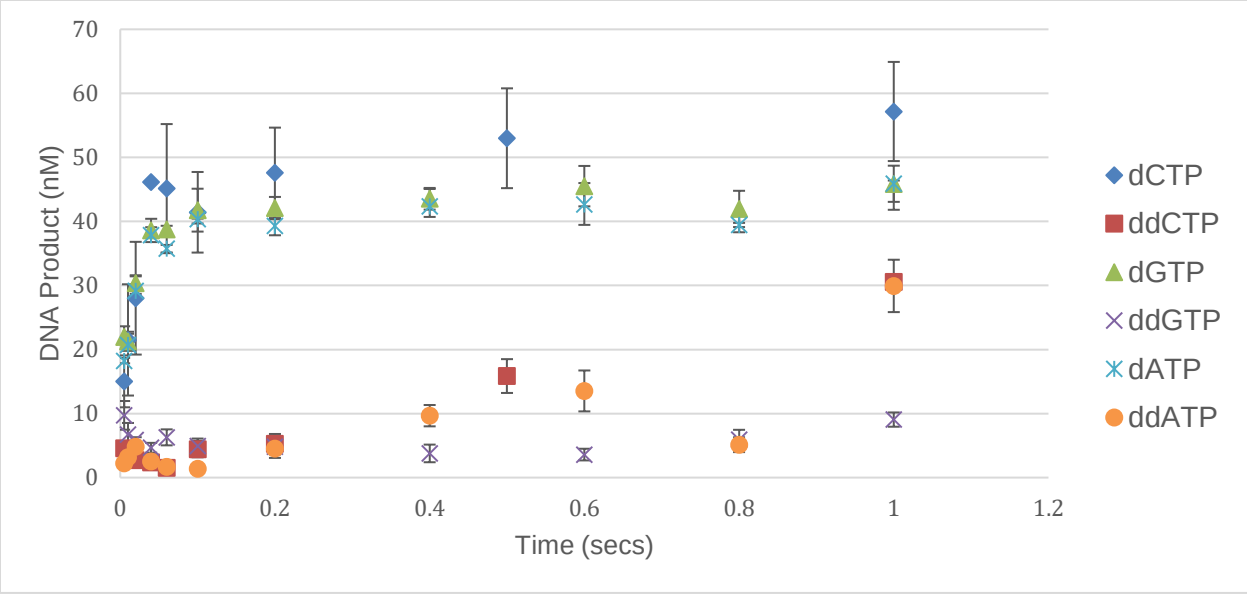

Figure #5 Pre-steady-state polymerization by MIP1 D347A comparing incorporation rates of dCTP (blue), ddCTP (red), dGTP (green), ddGTP (purple), dATP (teal), and ddATP (orange). Enzyme/DNA mix (75 nM Mip1, 250 nM DNA) was rapidly combined with Mg2+ and designated incoming nucleotide (50 µM), and reactions were quenched at the times indicated. Data were fit to the burst equation. The rates derived from the fitting of the burst equation are found in Table #3

Table #2 Constants Derived From Burst Equation Fitting Varying ddNTP

A_0	42.9	+/-	8.2	nM
v_{ss}	2.96	+/-	1.4	nM/s
k_{pol} (dATP)	80.9	+/-	1.0	s^{-1}
k_{pol} (dGTP)	84.3	+/-	21.1	s^{-1}
k_{pol} (dCTP)	56.2	+/-	37.6	s^{-1}
k_{pol} (ddATP)	0.74	+/-	0.17	s^{-1}
k_{pol} (ddGTP)	0.09	+/-	0.04	s^{-1}
k_{pol} (ddCTP)	0.91	+/-	0.21	s^{-1}
k_{off}	0.072	+/-	0.04	s^{-1}

The polymerase rate of ddCTP was assayed by replicating the pre-steady state assays performed on Mip1 D347A on exonuclease active Wt-Mip1, and the CTE deletion mutants (Mip1d175) with and without active exonuclease activity. Comparison of the pre-steady state polymerization rate between the Mip1 variants was used to determine if the CTE improves Mip1's ability to discriminate against ddNTPs. ddCTP was selected because it appeared to have the highest rate of misincorporation in the Mip1 D347A assays. The plot of the results and the resulting burst equation fitting constants are shown in Figure #6 and Table #3 respectively. These results appear to show that all Mip1 variants incorporate ddCTP at a slower rate than the control dCTP. Exonuclease activity did not appear to be a factor in these assays. However, the lack of detectable exonuclease activity could be a result of the rapid pre-steady state time course and the lack of experimental replications. The similar k_{pol} rates between Wt-MIP1 and MIP1d175 suggest that the CTE does not directly affect the polymerase reaction, and why the CTE did not affect the rate of ddCTP misincorporation. This does not rule out the possible CTE function in altering DNA or incoming nucleotide binding, similar to the function of the hPol γB accessory dimer[13]. DNA, dNTP, ddNTPs, and other NRTIs binding assays would be necessary to clarify any effect the CTE has on substrate binding. The current results suggest that the CTE and exonuclease sites of Mip1 are not a factor in ddNTP induced mtDNA chain termination.

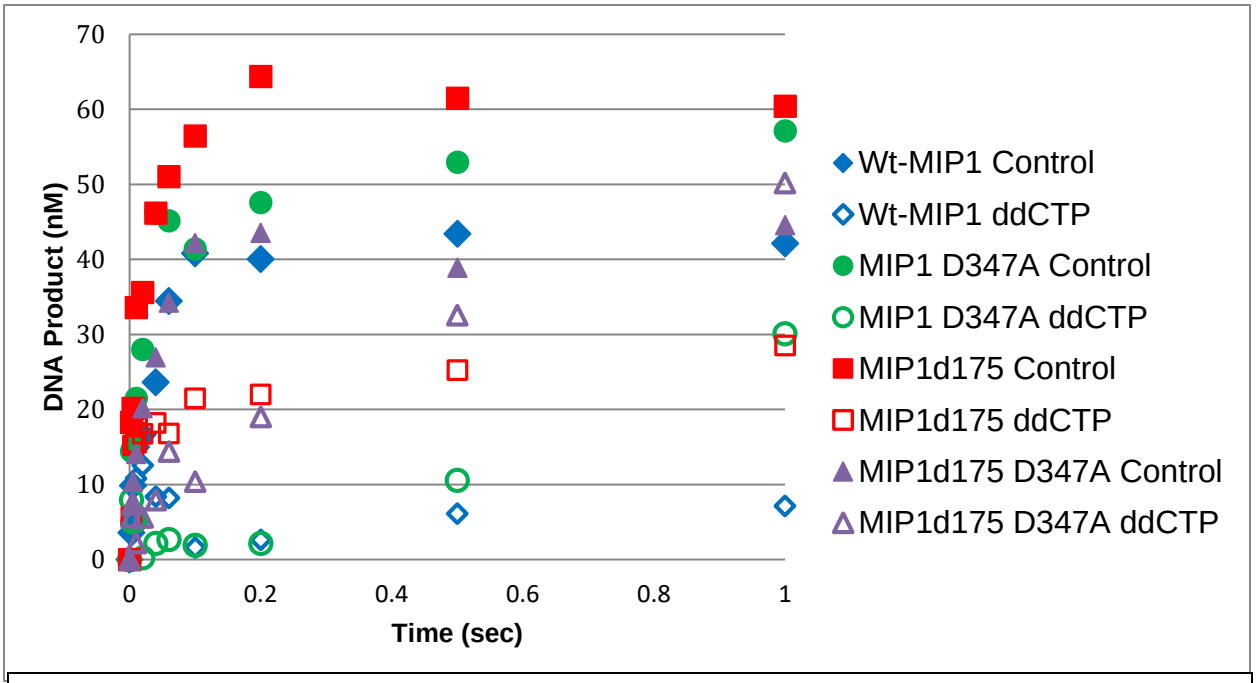

Figure #6 Pre-steady-state polymerization by WT-MIP1 (blue), MIP1 D347A (green), MIP1d175 (Red), and MIP1d175 D347A (purple) comparing incorporation rates of dCTP (solid) to ddCTP (hallow). Enzyme/DNA mix (75 nM Mip1, 250 nM DNA) was rapidly combined with Mg2+ and dCTP or ddCTP (50 µM), and reactions were quenched at the times indicated. Data were fit to the burst equation.

Table #3 Constants Derived From Burst Equation Fitting of Mip1 Variants

	A_0	v_{ss}	k_{obs} dCTP	k_{obs} ddCTP
Wt-MIP1	41.7	0.55	27.9	0.21
MIP1 D347A	42.9	2.95	56.2	0.91
MIP1d175	57.4	0.23	67.3	1.31
MIP1d175 D347A	41	2.32	33.9	3.63

Pre-steady state exonuclease activity suggest the CTE is unable to support the removal of incorporated ddCTP: Wt-Mip1 was assayed to determine if the polymerases' less discriminating exonuclease activity could remove ddNTPs that had been misincorporated where hPol γ could not[45]. Pre-steady state burst activity assays were performed on DNA complex that possessed a Watson-Crick base pair match or mismatch comparing those with or without a 3'OH group. These DNA constructs effectively model the conditions seen when either a dNTP or a ddNTP have been incorporated or misincorporated. The plot of the results is shown in Figure #7. Mip1 struggled to remove the ddCTP. The assays run on DNA lacking the 3' OH group showed the least amount of exonuclease activity. The direct comparison of the control matched vs. control mismatched suggested that Mip1's exonuclease site is more discerning in the pre-steady state. Experiments were then run to compare the full length and CTE deletion variants to determine if the CTE may alter Mip1 ability to remove ddCTP. The results suggest that the CTE does not affect the exonuclease reaction. This suggests that the specific chemistry found in the exonuclease active site is conserved between Mip1 and hPol γ.

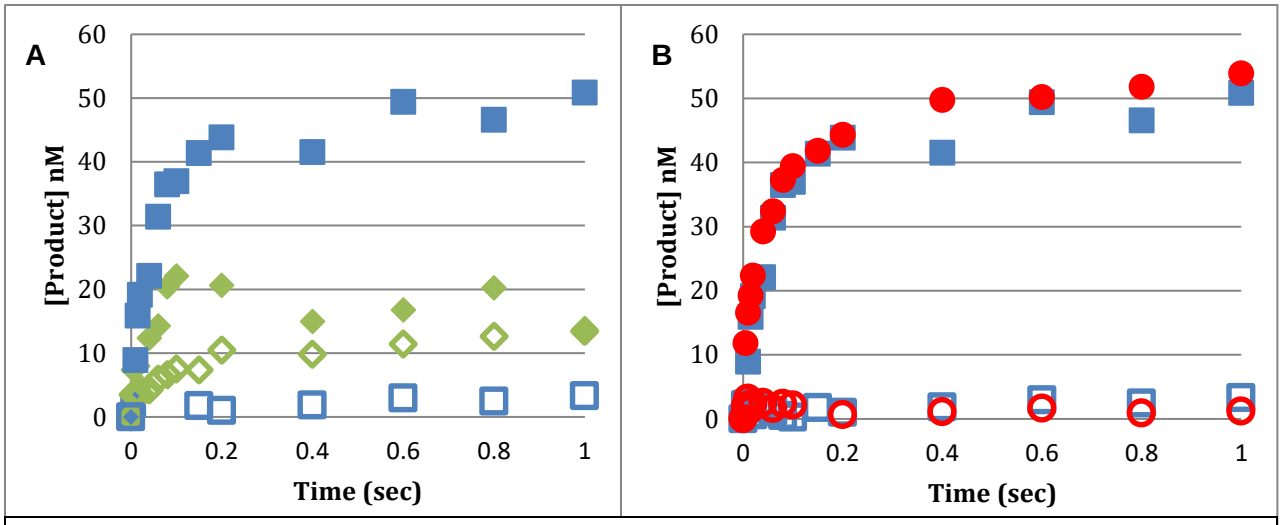

Figure #7: Pre-steady-state exonuclease activity assays. (A) Wt-Mip1 comparing excision rates of Watson-Crick Matched base pair (solid green), mismatched base pair (solid blue), matched ddCTP (hollow green), and mismatched ddCTP terminated DNA (hollow blue). The exonuclease activity readily removed the mismatched dCTP while struggling to rapidly remove the ddCTP and correctly matched bases. (B) Comparison of the rate of excision of mismatched base that either had or was missing the 3' hydroxile with and without the CTE domain. Wt-Mip1 dCTP terminated DNA (solid blue), Wt-Mip1 on ddCTP termianted DNA (hollow blue), MIP1d175 on dCTP terminated DNA (solid red) and Mip1d175 on ddCTP terminated DNA (hollow red). Both the Wt and the MIP1d175 readily removed the mismatched base but struggled to excise the ddCTP.

Strand displacement assays suggest the initiation of strand displacement by Mip1 is influenced by the polymerase's exonuclease activity and the construct of the 5' end of the blocking strand of DNA. The potential function of Mip1's exonuclease active site on strand displacement ability was assayed using two different DNA constructs. The first construct used a DNA blocking strand containing 2 mismatched ntp to generate a small 5' flap on blocking DNA. The mismatch was used to create a minor flap, similar to those found when a replication fork collapses or during BER. The second DNA construct possessed a 5' blunt ended of perfectly matched DNA blocking the DNA template after an 8ntp gap. This construct simulates a potential DNA repair intermediate or when the

DNA polymerase approaches an origin of replication. The DNA sequencing gel results can be found in Figure #8.

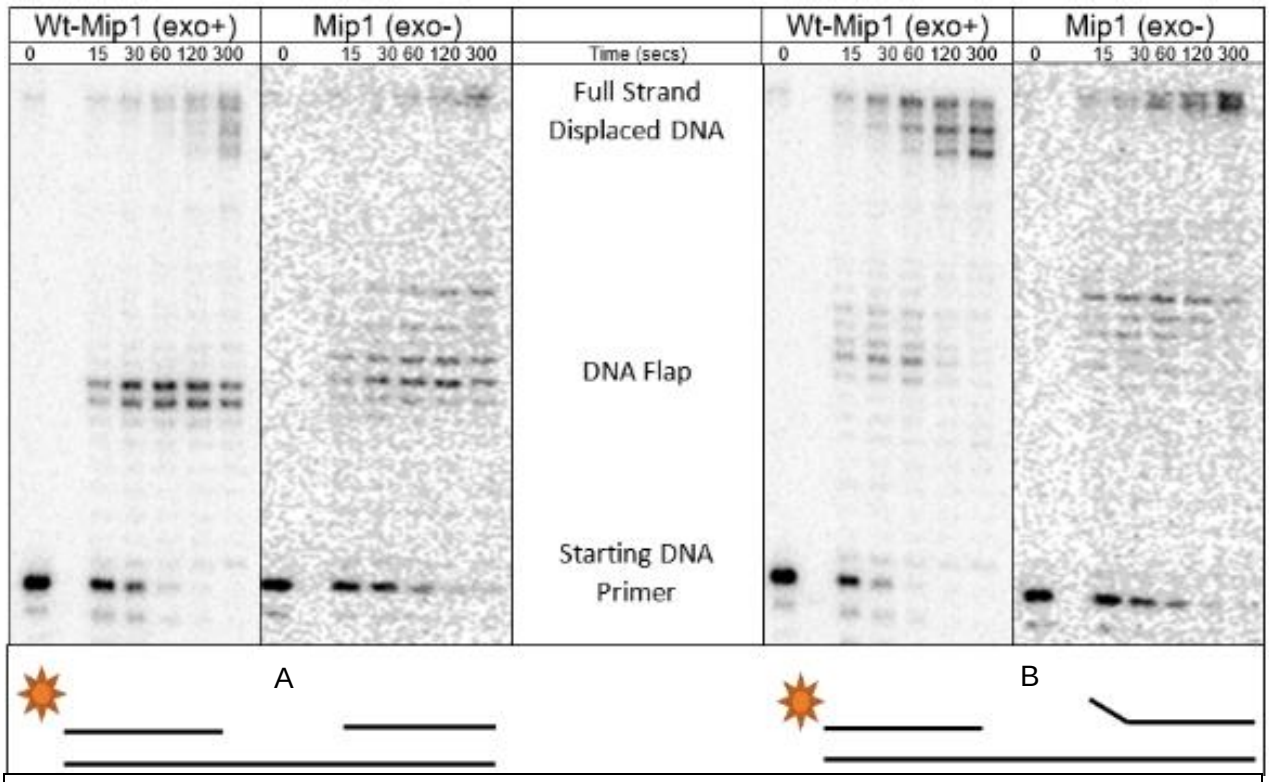

Figure #8 DNA sequencing gel images of steady state strand displacement experiment. (Left) Gels images of Mip1 extension on blunt DNA complex. The majority of the signal can be seen around the point where strand displacement would initiate. (Right) Gels images of Mip1 extension on flap DNA template. The majority of the signal if found in the final product, which required full strand displacement. Cartoons of the (A) blunt DNA complex and (B) flap DNA complex.

The first DNA construct with the short flap appears to be readily strand displaced by Mip1. This result agrees with what has already been reported on rolling circle assays. However, Mip1 appears to produce less fully strand displaced product when confronted with a perfectly matched 5' DNA strand. This suggests that Mip1 is able to distinguish between different 5' ends of blocking strand DNA. Mip1's ability to modulate strand displacement activity based upon the construct of the blocking DNA strand could be a deciding factor in the which method of BER is utilized.

The strand displacement assays were carried out using full length Mip1, with and without the exonuclease activity, to determine if Mip1 resembled hPol γ's. hPol γ requires the inactivation of the exonuclease domain to initiate strand displacement[46]. The elimination of the exonuclease activity would drive the protein in the polymerase direction exclusively, encouraging strand displacement. However, the exonuclease deficient Mip1 appeared to possess reduced strand displacement activity in direct contrast to what was observed with hPol γ. This raised the question of what function the 3' to 5' proof reading exonuclease site serves in the initiation of strand displacement. Specifically, could the exonuclease activity be required to initiate strand displacement needed for LP-BER or prevent overextension.

Mip1's ability to incorporate dNTPs and initiate strand displacement during BER was assayed on DNA constructs containing a ssDNA break of 0, 1, or 2 nucleotides The DNA sequencing gel results are shown in Figure #9. The shorter gap sizes resemble ssDNA breaks and intermediates found in BER. Similar to previous experiment with longer ssDNA gaps, the exonuclease active Mip1 was able to readily strand displace across all DNA constructs. That included the at the site of a single DNA nick where the very first incorporation would require strand displacement. In comparison, the exonuclease inactive Mip1 struggled to reach fully strand displaced product during the same time course. Mip1 (exo-) may not have reached full strand displacement, but it was able to readily incorporate into a gap of at least 1ntp. These results suggest that Mip1 prefers functioning in LP-BER, although the Mip1 (exo-) demonstrated an ability to function in the single nucleotide gap generated during SP-BER.

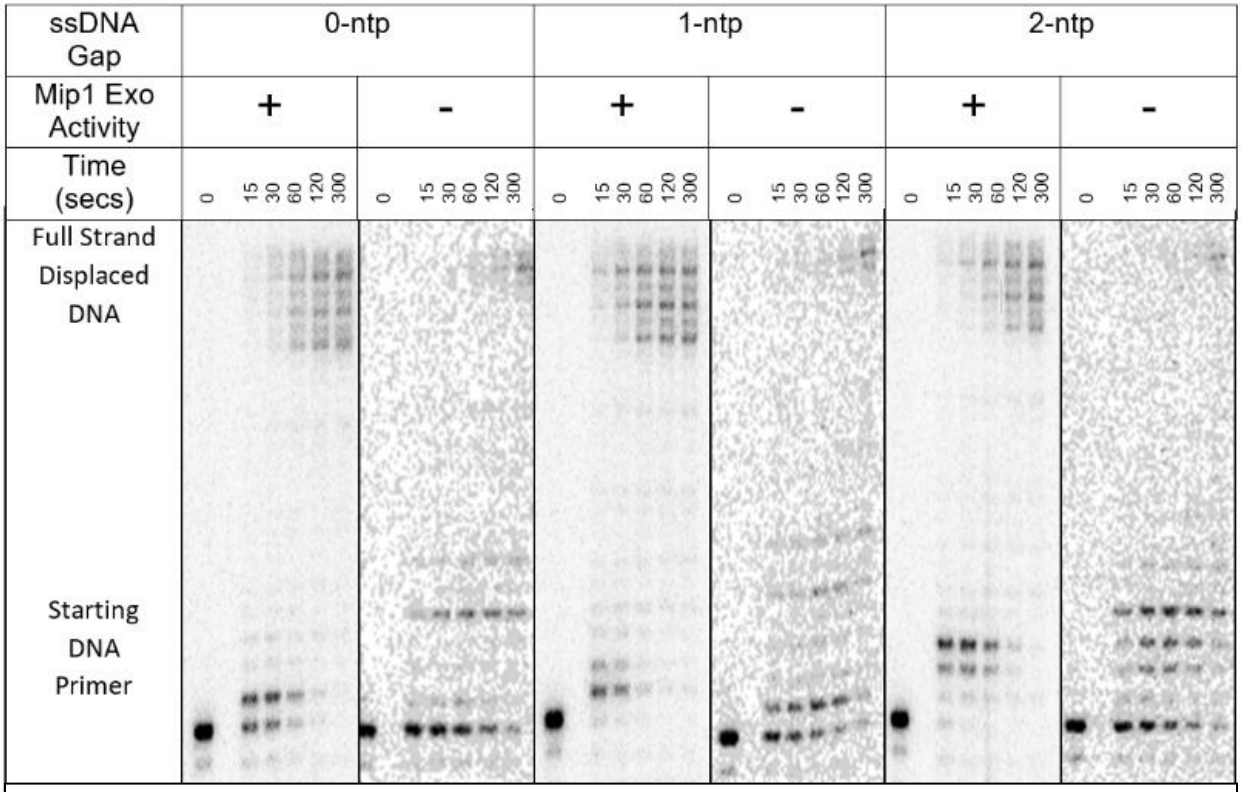

Figure #9 Strand displacement experiment determining if full length Mip1 is able to incorporate incoming nucleotides into 0, 1, or 2-ntp gaps similar to those found during BER. Both Mip1 variants were able to reach full length product, meaning the blocking DNA strand was completely displaced. However, the exonuclease active Mip1 was able to readily reach full extension and strand displacement. The exonuclease deficient Mip1 primarily stalled on the 0-ntp gap. Mip1 (exo-) was able to incorporate into the gaps between 1-2 ntps in length.

The ability to initiate full strand displacement from even a nick in DNA could cause accidental mtDNA replication during BER. Mip1's CTE may be important for regulating this activity to prevent unintended DNA replication since the CTE balances polymerase and exonuclease activity. *in vivo* the CTE may direct Mip1 towards the exonuclease deficient phenotype to reduce the rate of and length of strand displacement.

E. Discussion

Betaine is an important molecule for the stabilizing DNA binding proteins during protein expression and purification.

Expression and purification of active protein is critical for *in vitro* studies of enzymes. This process is often complicated by misfolding or aggregation of proteins, as seen in the original attempts to isolate active Mip1. Glycerol, which has long been used as a protein stabilizing agent for purification and long-term storage of proteins, failed to prevent the misfolding and aggregation of Mip1 protein. Betaine was selected as an alternative stabilizing agent because of its documented benefits stabilizing protein expression and crystallization[47] and improving polymerase function in PCR and DNA complex function[48,49]. Betaine is a small zwitter ionic molecule which appears to stabilize the structure of DNA binding proteins when the negatively charged DNA is unavailable during protein purification. Betaine may prove to be a valuable agent for proteins that are not well stabilized by glycerol.

Mip1 could be an ideal model for the study of the protein chemistry leading to NRTI induced toxicity.

The polymerase assays reported here suggest Mip1 incorporates ddNTP via a similar mechanism to what is seen in hPol γ. However, hPol γ experiences a significant increase in the affinity for ddNTPs that has not been tested for Mip1. This results in a net lack of discrimination against ddNTPs introduced to the polymerase as the increased binding affinity counteracts the decrease in incorporation rate[44]. There was a hope that the CTE and less discriminating exonuclease activity may have allowed Mip1 to remove

ddNTPs once misincorporated. However, the conservation of the polymerase and exonuclease reaction mechanisms demonstrated here support the use of Mip1 as a model for the study of NRTI induced toxicity. The study of Mip1 will provide more resources for understanding mitochondrial toxicity seen in some HIV patients treated with NRTIs.

The c-terminal domain of Mip1 is unique to the fungal mitochondrial polymerases and appears to possess its own distinct structure separate from the core polymerase structure. This separated CTE structure is similar to what is seen with the accessory proteins required by other mitochondrial DNA polymerases and even their close homolog T7 DNA polymerase[8,50]. The CTE slightly increases the processivity of Mip1 similar to the hPol γB dimer[11]. However, the CTE may serve additional functions similar to the accessory domains of hPol γ or T7 DNA polymerase. The current literature presents several potential theories for the function of Mip1 and the CTE, which can be refined based on the evidence presented here[18,51–55].

The C-terminal extension domain potentially functions as an activity inhibitor.

As single celled organisms, yeast lack significant survival tools found in complex multicellular organisms to deal with environmental challenges. Alcoholic fermentation provides a useful alternative by allowing yeast to survive periods of oxygen deprivation. The primary drawback is that alcoholic fermentation is far less efficient than OXPHO. Thus, alcoholic fermentation results in limited cellular energy that should not be wasted on the now unused mitochondria. The decrease in DNA binding affinity and polymerization rate of Mip1 possessing a CTE as reported by the Sedman lab could become beneficial under these circumstances[11]. The CTE provides a mechanism to

inhibit replication of the less critical mtDNA to preserve resources for the vital nuclear genome during anaerobic respiration. If conditions are severe enough, for long enough, the CTE may then be able activate Mip1's indiscriminate exonuclease function to begin digesting mtDNA; freeing dNMPs for phosphorylation and use in nuclear genome.

The loss of Mip1 functionality in the presence of the CTE should have resulted in the loss of this activity unless it provided some form of evolutionary advantage. This theory provides a mechanism for evolutionary selection retaining the apparent activity inhibiting CTE domain. This theory would also help explain Mip1's less discriminate exonuclease activity. Additional research into Mip1 and any potential associated or regulating factors would be required to confirm this theory.

Mip1 appears to prefer long-patch BER but possesses the ability to incorporate in a single ntp break required for short-patch BER.

The single nucleotide gap provided a functional intermediate generated during short-patch BER. This 1-ntp gap would occur after a DNA glycosylase and AP lyase have removed the single damaged base. The strand displacement experiments conducted here demonstrated that Mip1's was able to identify and fill a single nucleotide gap in DNA. However, only the exonuclease deficient Mip1 stopped after a single incorporation. While this could be a result of the lack of associated BER proteins that would be present *in vivo,* the initiation of strand displacement by exonuclease active Mip1 on all gap DNA constructs suggests that LP-BER is the preferred method of yeast mitochondria. This theory is supported by the evidence that the exonuclease deficient Mip1 appeared to stall after 4 incorporations, directly in the middle of the 2-7 nucleotide incorporations typical of LP-BER.

Mip1 could function as both the DNA helicase and DNA polymerase during mtDNA replication.

In humans, mtDNA replication requires the formation of a T7-like replisome made up of three proteins. (1) A DNA polymerase (hPol γ) for extension of the new DNA. (2) Mitochondrial single stranded binding proteins which stabilize the single stranded lagging DNA strand. (3) A DNA helicase (TWINKLE) for unwinding of the DNA duplex[56–58]. Unlike the nuclear replicating helicase, TWINKLE is unable to unwind duplexed DNA without the functional hPol γ even though it hydrolyzes ATP[59,60].

S. cerevisiae appears to be missing one of these key components. No replicating DNA helicase homologous to human TWINKLE has been found in the mitochondria of yeast. This suggests that yeast require an alternative method for displacing the non-template DNA strand. The experiments presented in this thesis demonstrate that Mip1 can initiate and perform extensive strand displacement independent of any other proteins on a variety of DNA constructs. This suggests a mechanism where Mip1 functions as both the replicating DNA polymerase and the helicase. This theory would also help explain why the human mtDNA replisome has coupled the strand displacing helicase activity with the polymerase reaction. *In vivo,* the coupling of polymerase and helicase into a single protein would be practical for yeast surviving via alcoholic fermentation when ATP required by DNA helicases would be limited. The requirement for Mip1 to function in place of a helicase may also influence Mip1's preference for LP-BER. This theory would significantly benefit from additional study of any potential effect the CTE may play in the initiation and regulation of Mip1's strand displacement ability.

Mip1's Combined Role in replication and repair could explain the various forms of mtDNA found in S. cerevisiae.

As discussed in the introduction, the mitochondrial genome of yeast are not uniformly present as the circular genomes found in humans. The discovery of linear DNA several mitochondrial genome units in length have caused the generation of two theories regarding replication in yeast[25]. (1) The most accepted theory proposes that replication begins at several origin (ORI) sites by RNA-primed bidirectional replication similar to that of chromosomal DNA[18]. (2) Replication is initiated by homologous recombination and strand invasion. The second theory then proposes that replication proceeds via a "rolling circle" mechanism to produce the linear DNA strands multiple genomes in length. These long linear fragments are then cut and circularized [26,53,61,62].

The evidence presented in this thesis suggests that these two theories do not need to be mutually exclusive. The multifunctionality of Mip1 provides potential mechanisms for both theories. If Mip1 functions in unwinding of mtDNA duplex for replication as suggested here, then Mip1 would be capable of initiating replication anywhere on the mitochondrial genome. That would suggest a third method for yeast mtDNA replication. The strand displacement experiments on BER intermediates suggest Mip1 may initiate replication spontaneously from a site of LP-BER repair. The unifying factor is the "rolling circle" mechanism. This mechanism explains the generation of the multiple genome long mtDNA fragments. At the opposite end of the spectrum, Mip1's exonuclease activity and potential ability to mistakenly initiate mtDNA replication could explain the truncated or damaged mtDNA found in *rho*$^{-}$ colonies.

In conclusion, Mip1 is a complex multifunctional protein critical for the maintenance of the mitochondrial genome of *S. cerevisiae.* Mip1 can participate in either short-patch or long-patch base excision repair depending on its exonuclease activity. Mip1's strand displacement ability could facilitate initiation of a replication fork from something as small as a single strand DNA break without the need for a dedicated DNA helicase. Despite all of these additional functions, Mip1 appears to have conserved all of the functions of its human ortholog, hPol γ. This makes Mip1 the perfect model for further studying mechanisms involved in the initiation of mtDNA replication, the selecting SP or LP-BER, and NRTI induced toxicity.

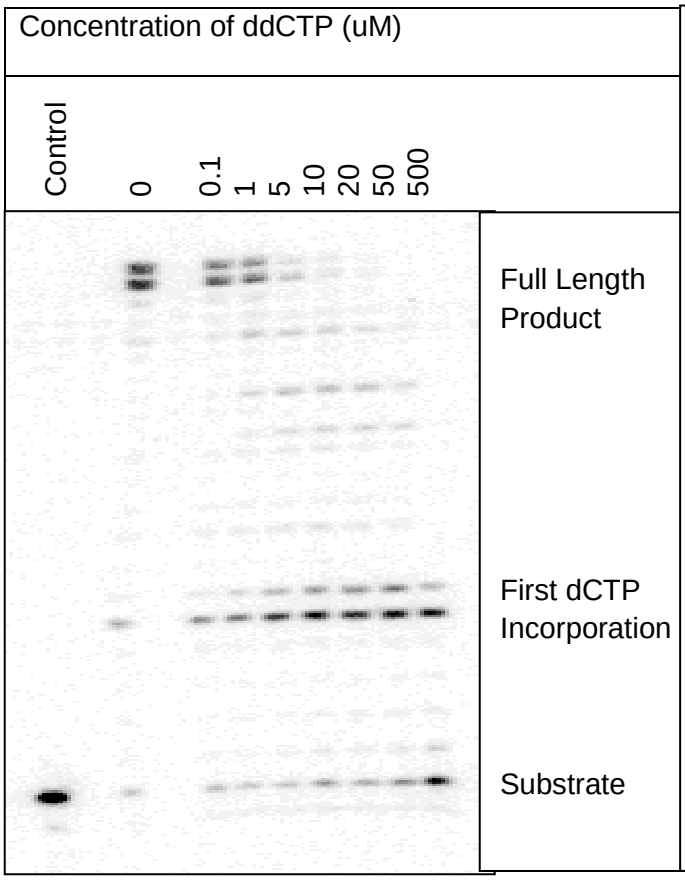

Appendix Figure #1: Steady state ddCTP competition assay was run using the same protocol detailed in the strand displacement experiments detailed above. Reactions were quenched after 30 seconds. Final reaction conditions; 100nM FL-MIP1, 250nM DNA complex, 10mM $MgCl_2$, 10uM dNTP mix, 25mM HEPES pH 7.5, 140mM NaCl, 0.2mg/ml BSA, 2mM 2-ME with the indicated concentration of ddNTP.

The competition assay titrating in ddCTP was used to determine if Mip1 would misincorporate ddNTPs similar to what has been demonstrated with hPol γ. The increase of the signal at the first dCTP incorporation site on the DNA template suggests that Mip1 is incorporating the ddCTP. The decrease in fully extended product supports this conclusion. The Watson-Crick base pairing appears to be important for ddNTP misincorporation.

F. References

1. Mager, W. H. & Winderickx, J. Yeast as a model for medical and medicinal research. *Trends Pharmacol. Sci.* **26,** 265–273 (2005).
2. Nass, M. M. K. & Nass, S. INTRAMITOCHONDRIAL FIBERS WITH DNA CHARACTERISTICS. *J. Cell Biol.* **19,** 593–611 (1963).
3. Eleutherio, E. *et al.* Oxidative stress and aging: Learning from yeast lessons. *Fungal Biol.* **122,** 514–525 (2018).
4. Goldring, E. S., Grossman, L. I. & Marmur, J. Petite Mutation in Yeast. *Journal of Bacteriology* **107,** 377–381 (1971).
5. Bernardi, G. The petite mutation in yeast. *Trends Biochem. Sci.* **4,** 197–201 (1979).
6. Schweyen, R. J. & Kaudewitz, F. On the formation of rho− petites in yeast. *Mol. Gen. Genet. MGG* **149,** 311–322 (1976).
7. Lee, Y.-S., Kennedy, W. D. & Yin, Y. W. Structural insight into processive human mitochondrial DNA synthesis and disease-related polymerase mutations. *Cell* **139,** 312–324 (2009).
8. Lee, Y.-S. *et al.* Each monomer of the dimeric accessory protein for human mitochondrial DNA polymerase has a distinct role in conferring processivity. *J. Biol. Chem.* **285,** 1490–1499 (2010).
9. Sohl, C. D. *et al.* Probing the structural and molecular basis of nucleotide selectivity by human mitochondrial DNA polymerase γ. *Proc. Natl. Acad. Sci.* **112,** 8596–8601 (2015).
10. Szymanski, M. R. *et al.* Structural basis for processivity and antiviral drug toxicity in human mitochondrial DNA replicase. *EMBO J.* **34,** 1959–1970 (2015).
11. Viikov, K., Jasnovidova, O., Tamm, T. & Sedman, J. C-terminal extension of the yeast mitochondrial DNA polymerase determines the balance between synthesis and degradation. *PLoS One* **7,** e33482 (2012).
12. Viikov, K., Valjamae, P. & Sedman, J. Yeast mitochondrial DNA polymerase is a highly processive single-subunit enzyme. *Mitochondrion* **11,** 119–126 (2011).
13. Johnson, A. A., Tsai, Y., Graves, S. W. & Johnson, K. A. Human Mitochondrial DNA Polymerase Holoenzyme : Reconstitution and. 1702–1708 (2000).
14. Barja, G. & Herrero, A. Oxidative damage to mitochondrial DNA is inversely related to maximum life span in the heart and brain of mammals. *FASEB J.* **14,** 312–318 (2000).
15. Robertson, A. B., Klungland, A., Rognes, T. & Leiros, I. DNA repair in mammalian cells: Base excision repair: the long and short of it. *Cell. Mol. Life Sci.* **66,** 981–993 (2009).
16. Prakash, A. & Doublie, S. Base Excision Repair in the Mitochondria. *J. Cell. Biochem.* **116,** 1490–1499 (2015).
17. Demple, B. & DeMott, M. S. Dynamics and diversions in base excision DNA repair

of oxidized abasic lesions. *Oncogene* **21,** 8926–8934 (2002).
18. Lecrenier, N. & Foury, F. New features of mitochondrial DNA replication system in yeast and man. *Gene* **246,** 37–48 (2000).
19. Perna, A. *et al.* Different Cell Cycle Modulation in SKOV-3 Ovarian Cancer Cell Line by Anti-HIV Drugs. *Oncol. Res.* **25,** 1617–1624 (2017).
20. Carlini, F. *et al.* The reverse transcription inhibitor abacavir shows anticancer activity in prostate cancer cell lines. *PLoS One* **5,** e14221 (2010).
21. Johnson, A. A. *et al.* Toxicity of antiviral nucleoside analogs and the human mitochondrial DNA polymerase. *J. Biol. Chem.* **276,** 40847–40857 (2001).
22. Chattopadhyay, K. & Aldous, C. A brief review on human mtDNA mutations and NRTI-associated mtDNA toxicity and mutations. *Mitochondrial DNA. Part A, DNA mapping, Seq. Anal.* **27,** 1685–1687 (2016).
23. White, A. Mitochondrial toxicity and HIV therapy. *Sexually Transmitted Infections* **77,** 158–173 (2001).
24. Lodi, T. *et al.* DNA polymerase gamma and disease: what we have learned from yeast. *Front. Genet.* **6,** 106 (2015).
25. Maleszka, R., Skelly, P. J. & Clark-Walker, G. D. Rolling circle replication of DNA in yeast mitochondria. *EMBO J.* **10,** 3923–3929 (1991).
26. Ling, F. & Shibata, T. Recombination-dependent mtDNA partitioning: in vivo role of Mhr1p to promote pairing of homologous DNA. *EMBO J.* **21,** 4730–4740 (2002).
27. Cheng, X. & Ivessa, A. S. Association of the yeast DNA helicase Pif1p with mitochondrial membranes and mitochondrial DNA. *Eur. J. Cell Biol.* **89,** 742–747 (2010).
28. Ramachandran, A. *et al.* The Yeast Mitochondrial RNA Polymerase and Transcription Factor Complex Catalyzes Efficient Priming of DNA Synthesis on Single-stranded DNA. *J. Biol. Chem.* **291,** 16828–16839 (2016).
29. Michikawa, Y., Mazzucchelli, F., Bresolin, N., Scarlato, G. & Attardi, G. Aging-dependent large accumulation of point mutations in the human mtDNA control region for replication. *Science* **286,** 774–779 (1999).
30. Hsu, C.-C., Tseng, L.-M. & Lee, H.-C. Role of mitochondrial dysfunction in cancer progression. *Exp. Biol. Med. (Maywood).* **241,** 1281–1295 (2016).
31. Tan, D.-J., Bai, R.-K. & Wong, L.-J. C. Comprehensive scanning of somatic mitochondrial DNA mutations in breast cancer. *Cancer Res.* **62,** 972–976 (2002).
32. Mecocci, P., MacGarvey, U. & Beal, M. F. Oxidative damage to mitochondrial DNA is increased in Alzheimer's disease. *Ann. Neurol.* **36,** 747–751 (1994).
33. Gui, Y.-X., Xu, Z.-P., Lv, W., Zhao, J.-J. & Hu, X.-Y. Evidence for polymerase gamma, POLG1 variation in reduced mitochondrial DNA copy number in Parkinson's disease. *Parkinsonism Relat. Disord.* **21,** 282–286 (2015).
34. Corral-Debrinski, M., Shoffner, J. M., Lott, M. T. & Wallace, D. C. Association of

mitochondrial DNA damage with aging and coronary atherosclerotic heart disease. *Mutat. Res.* **275,** 169–180 (1992).
35. Komulainen, T. *et al.* Mitochondrial DNA Depletion and Deletions in Paediatric Patients with Neuromuscular Diseases: Novel Phenotypes. *JIMD Rep.* **23,** 91–100 (2015).
36. Foury, F. & Vanderstraeten, S. Yeast mitochondrial DNA mutators with deficient proofreading exonucleolytic activity. *EMBO J.* **11,** 2717–2726 (1992).
37. D., S., C., B. & J., K. M. H. CRYSOL– a Program to Evaluate X-ray Solution Scattering of Biological Macromolecules from Atomic Coordinates. *J. Appl. Crystallogr.* **28,** 768–773
38. V., K. P., V., V. V., V., S. A., J., K. M. H. & I., S. D. PRIMUS: a Windows PC-based system for small-angle scattering data analysis. *J. Appl. Crystallogr.* **36,** 1277–1282
39. Petoukhov, M. V & Svergun, D. I. Ambiguity assessment of small-angle scattering curves from monodisperse systems. *Acta Crystallogr. D. Biol. Crystallogr.* **71,** 1051–1058 (2015).
40. Baugh, E. H., Lyskov, S., Weitzner, B. D. & Gray, J. J. Real-time PyMOL visualization for Rosetta and PyRosetta. *PLoS One* **6,** e21931 (2011).
41. Bender, M. L. *et al.* The determination of the concentration of hydrolytic enzyme solutions: alpha-chymotrypsin, trypsin, papain, elastase, subtilisin, and acetylcholinesterase. *J. Am. Chem. Soc.* **88,** 5890–5913 (1966).
42. Kroutil, O., Romancová, I., Šíp, M. & Chval, Z. Cy3 and Cy5 Dyes Terminally Attached to 5′C End of DNA: Structure, Dynamics, and Energetics. *J. Phys. Chem. B* **118,** 13564–13572 (2014).
43. Ouellet, J., Schorr, S., Iqbal, A., Wilson, T. J. & Lilley, D. M. Orientation of Cyanine Fluorophores Terminally Attached to DNA via Long, Flexible Tethers. *Biophysical Journal* **101,** 1148–1154 (2011).
44. Feng, J. Y., Johnson, A. A., Johnson, K. A. & Anderson, K. S. Insights into the Molecular Mechanism of Mitochondrial Toxicity by AIDS Drugs. *J. Biol. Chem.* **276,** 23832–23837 (2001).
45. Lim, S. E. & Copeland, W. C. Differential Incorporation and Removal of Antiviral Deoxynucleotides by Human DNA Polymerase γ. *J. Biol. Chem.* **276,** 23616–23623 (2001).
46. He, Q., Shumate, C. K., White, M. A., Molineux, I. J. & Yin, Y. W. Exonuclease of human DNA polymerase gamma disengages its strand displacement function. *Mitochondrion* **13,** 592–601 (2013).
47. Oganesyan, N., Ankoudinova, I., Kim, S.-H. & Kim, R. Effect of Osmotic Stress and Heat Shock in Recombinant Protein Overexpression and Crystallization. *Protein expression and purification* **52,** 280–285 (2007).
48. Rees, W. A., Yager, T. D., Korte, J. & Von Hippel, P. H. Betaine can eliminate the

base pair composition dependence of DNA melting. *Biochemistry* **32,** 137–144 (1993).
49. Henke, W., Herdel, K., Jung, K., Schnorr, D. & Loening, S. A. Betaine improves the PCR amplification of GC-rich DNA sequences. *Nucleic Acids Res.* **25,** 3957–3958 (1997).
50. Mark, D. F. & Richardson, C. C. Escherichia coli thioredoxin: a subunit of bacteriophage T7 DNA polymerase. *Proceedings of the National Academy of Sciences of the United States of America* **73,** 780–784 (1976).
51. Roganti, T. & Lecrenier, N. The complete sequence of the mitochondrial genome of Saccharomyces cerevisiae è ne. **440,** 325–331 (1998).
52. Shibata, T. & Ling, F. DNA recombination protein-dependent mechanism of homoplasmy and its proposed functions. *Mitochondrion* **7,** 17–23 (2007).
53. Gerhold, J. M., Aun, A., Sedman, T., Joers, P. & Sedman, J. Strand invasion structures in the inverted repeat of Candida albicans mitochondrial DNA reveal a role for homologous recombination in replication. *Mol. Cell* **39,** 851–861 (2010).
54. Brown, T. A., Cecconi, C., Tkachuk, A. N., Bustamante, C. & Clayton, D. A. Replication of mitochondrial DNA occurs by strand displacement with alternative light-strand origins , not via a strand-coupled mechanism. 2466–2476 (2005). doi:10.1101/gad.1352105.other
55. Holt, I. J. & Reyes, A. Human mitochondrial DNA replication. *Cold Spring Harb. Perspect. Biol.* **4,** (2012).
56. McKinney, E. & Oliveira, M. Replicating animal mitochondrial DNA. *Genet. Mol. Biol.* **315,** 308–315 (2013).
57. Miralles Fuste, J. *et al.* In vivo occupancy of mitochondrial single-stranded DNA binding protein supports the strand displacement mode of DNA replication. *PLoS Genet.* **10,** e1004832 (2014).
58. Sen, D., Nandakumar, D., Tang, G. Q. & Patel, S. S. Human mitochondrial DNA helicase TWINKLE is both an unwinding and annealing helicase. *J. Biol. Chem.* **287,** 14545–14556 (2012).
59. Korhonen, J. A., Pham, X. H., Pellegrini, M. & Falkenberg, M. Reconstitution of a minimal mtDNA replisome in vitro. *EMBO J.* **23,** 2423–2429 (2004).
60. Korhonen, J. A., Gaspari, M. & Falkenberg, M. TWINKLE Has 5’ -> 3’ DNA helicase activity and is specifically stimulated by mitochondrial single-stranded DNA-binding protein. *J. Biol. Chem.* **278,** 48627–48632 (2003).
61. Ling, F., Hori, A. & Shibata, T. DNA Recombination-Initiation Plays a Role in the Extremely Biased Inheritance of Yeast [rho-] Mitochondrial DNA That Contains the Replication Origin ori5. *Mol. Cell. Biol.* **27,** 1133–1145 (2007).
62. Milenkovic, D. *et al.* Twinkle is an essential mitochondrial helicase required for synthesis of nascent D-loop strands and complete mtDNA replication. *Hum. Mol. Genet.* **22,** 1983–1993 (2013).